SAPIENZA
UNIVERSITÀ DI ROMA

Department of Translation Medicine and Precision

PhD in

"Arterial Hypertension And Vascular Biology"

XXXV Cycle

Coordinator: Prof. Claudio Letizia

PhD Thesis

"MYOCARDIAL ALDOSTERONE RECEPTORS AND AQUAPORIN 1 UP-REGULATION CAUSING CARDIOMYOCYTE REMODELING IN HUMAN HEART FAILURE"

PhD Student **Tutor**

Maria Alfarano, MD **Prof.ssa Cristina Chimenti**

Summary

Introduction

Cardiomyopathies are heterogeneous disorders characterized by structural and functional abnormalities of the myocardium, not explained solely by coronary artery disease or abnormal loading conditions.

In last decades, several studies have confirmed that aldosterone is important in the pathophysiology of heart failure, and in large series of clinical studies (Rales [1], Emphasis-HF [2,3] and Ephesus [4]) specific blockade of aldosterone receptors substantially reduced the risk of progressive heart failure, hospitalization and death. As consequence, aldosterone inhibitors are recommended by the current guidelines treatment of heart failure (5,6). However, the cellular and molecular mechanisms by which these drugs determine clinical improvement is unknown so far. In the heart, aldosterone may act as enhancer of hypertrophic response and excessive stimulation of the mineralcorticoid receptor can induce cell death.

A previous report has demonstrated that primary aldosteronism-associated cardiomyopathy (7) is characterized by prominent myocardial hypertrophy and fibrosis, with water accumulation in cytosol and organelles of cardiomyocytes and microvascular smooth muscle cells, associated to reduced myofibril concentration and increase of myocardial aldosterone receptors (AR) and aquaporin-1 (AQ1). Removal of hypersecreting adrenal adenoma and normalization of plasma aldosterone levels is associated with reduction of cardiomyocyte diameter and disappearance of intracellular vacuoles, recovery of electron-density of cytosol and cell organelles and myofibrillar content. Furthermore down-regulation of aldosterone receptors and aquaporin 1 channels, with myocardial mass reduced, is associated to recovery of cardiac contractility. Thus, primary aldosteronism-

associated cardiomyopathy is a reversible entity characterized by an overexpression of myocardial aldosterone receptors and aquaporin-1 channels, with cardiomyocyte and microvascular water accumulation, maladaptive hypertrophy, areas of myofibrillolysis, and the impairment of myocyte relaxation and contraction; all these changes are reversed after definitive treatment of aldosterone excess, highlighting direct effects of aldosterone excess on development of cardiac changes.

Therefore, we thought to characterize the morpho-molecular changes of cardiomyocytes that accompany human heart failure. In fact, the effects of secondary aldosteronism on aldosterone and aquaporin myocyte receptors and their consequences on cardiac cell composition and function are still unknown.

Aim of the present study is to evaluate the cardiomyocyte AR and AQ1 expression in human failing heart and after recovery and their influence on cell composition and function.

Myocardial Aldosterone Receptors and Aquaporins

Mineralcorticoid antagonists (MRAs) are established in the treatment of heart failure with reduced ejection fraction and they improve both survival and quality of life, through modulation of myocardial fibrosis (8). It has been demonstrated that aldosterone, by binding to the mineralocorticoid receptor, causes inflammation and fibrosis of the heart, fibrosis and remodelling of blood vessels and tubulointerstitial fibrosis and glomerular injury in the kidney (9). In rats, infusion of aldosterone plus saline load causes inflammation of the myocardium which results in fibrosis (10). These effects of aldosterone are prevented by MRAs with beneficial effects in term of reduction of progressive heart failure, hospitalization and death as demonstrated in several trials such as Rales (1), Emphasis-HF (2,3) and Ephesus (4), on the basis of which MRAs have been recommended in the heart failure guidelines. In the Randomized Aldactone Evaluation Study (RALES), spironolactone reduced mortality in heart failure patients who were already being treated with standard therapy including an angiotensin-converting-enzyme inhibitor. In the Eplerenone in Mild Patients Hospitalization and Survival Study in Heart Failure (EMPHASIS-HF), the aldosterone antagonism was also beneficial in patients with chronic heart failure and mild symptoms. In the Eplerenone Post-Acute Myocardial Infarction Heart Failure Efficacy and Survival Study (EPHESUS), eplerenone treatment reduced mortality and hospitalization in patients with left ventricular dysfunction following myocardial infarction.

High levels of aldosterone induce myocardial hypertrophy through two different mechanisms: increase of sarcomere mass by a pro-hypertrophic effect mediated

by a G- protein coupled receptor kinase 5 cytosolic signaling (11) and retention of ions and water regulated by nuclear receptor-dependent gene expression of ion channel, transporters and aquaporins (12). Aquaporins (AQs) are a group of proteins with high-selective permeability for water, expressed in many organs and tissue. AQPs are expressed constitutively in cell membranes or stored in membrane bound vesicles within the cytoplasm and moved into an active position within the cell membrane in response to a hypertonic stimulus, allowing bidirectional flow of water. In the heart are expressed aquaporin-1 and aquaporin-4. Its expression is osmo-dependent (13). Aquaporin-1 is highly expressed in the cytoplasm of cardiomyocytes, smooth muscle cells and endothelial cells (7). Water accumulation in the myocardium is correlated with contractility changes and myocardial dysfunction (14).

Myocardial expression of aldosterone receptor and cardiac aquaporin have impact on water homeostasis and energy balance and play a crucial role in normal and pathophysiological cardiac function; elevated values in heart failure are correlated with myocardial dysfunction. However, the morpho-molecular changes of cardiomyocytes that accompany human heart failure are still uninvestigated.

The Study: Myocardial Aldosterone Receptors and Aquaporin 1 Up-regulation Causing Cardiomyocyte Remodeling in Human Heart Failure.

Abstract

Background: Abnormal aldosterone signaling is a recognized source of cardio-vascular damage. Its influence on cardiomyocyte structure, function and hormonal receptors when associated with heart failure is still unreported.

Methods: Twenty-six consecutive patients with heart failure (LVEF < 40%), normal coronaries and valves, underwent a left ventricular endomyocardial biopsy (EMB) for evaluation of myocardial substrate. Biopsy samples were processed for histology, electron microscopy, immunohistochemistry, and Western Blot analysis of myocardial aldosterone receptors and aquaporin-1 correlated with plasma aldosterone (AD) and renin activity (PRA). Eight patients with virus-negative inflammatory cardiomyopathy (ICM), had a control EMB after 6 months of immunosuppressive therapy and recovery of cardiac function with re-evaluation of cardiomyocyte structure and receptor expression.

Results: EMB in addition to the diagnosis of myocarditis (15 cases), dilated cardiomyopathy (CM, 6), alcohol CM (2), diabetic CM (3), showed vacuolar degeneration and cloudy swelling of cardiomyocytes corresponding at electron microscopy to ions and water accumulation into cytosol**,** membrane-bound vesicles, nucleus and other organelles, associated to an increased AD, PRA and myocardial expression of aldosterone receptors (2.3 fold) and aquaporin 1 (2.6 fold). In the 8 pts recovered from ICM, cardiomyocyte diameter reduced with disappearance of intracellular vacuoles, normalization of cytosol, nucleus and cell organelles' electron-density, along with down-regulation of aldosterone receptors and aquaporin-1.

Conclusion: Human heart failure is associated with over-expression of myocyte aldosterone receptors and aquaporin-1 causing intracellular water overloading, swelling and functional compromise of cardiomyocytes. Cardiac recovery is accompanied by down-regulation of hormonal receptors and normalization of cell structure and composition.

Key words: hyperaldosteronism, myocardial damage, heart failure, aldosterone receptors, aquaporin-1, vacuolar degeneration, cloudy swelling, cell volume control, cellular and molecular rehabilitation.

Methods

Patient population

Twenty-six consecutive patients with dilated cardiomyopathy and left ventricular dysfunction (LVEF < 40%), that from January 2019 to December 2019 underwent a left ventricular endomyocardial biopsy study for morphomolecular characterization of myocardial substrate (15), represented our patient population. All patients were on treatment on heart failure treatment but aldosterone inhibitors. Among them 15 patients received a diagnosis of virus-negative inflammatory cardiomyopathy, 6 had a non-familiar idiopathic dilated cardiomyopathy, 2 (with a history of addiction) had alcoholic cardiomyopathy and the remaining 3 a diabetic cardiomyopathy correlated to a long history of diabetes.

Fifteen patients with virus-negative inflammatory cardiomyopathy received a six-month treatment with immunosuppression according with TIMIC protocol (16). Eight of them with cardiac recovery accepted to have a control EMB at the end of the treatment.

Biochemical measurements

Fasting blood samples for plasma aldosterone concentration (PAC) and plasma renin activity (PRA) were obtained in all patients. Patients were comfortably lying in a clinostatic position for at least half an hour. The assay for aldosterone (PAC) was performed with the diagnostic kits (Aldosterone Mirya; Technogenetics, Sesto, Italy). Normal ranges were 10–150 pg/ml supine and 30–320 pg/ml upright on a normal Na diet; intraassay and interassay coefficients of variation were both less than 5.6%, and the cross-reactivity of the antibody for aldosterone for other

adrenal steroids was less than 0.001%. PRA was measured by radioimmunoassay (RIA) using commercial kits (Ren CTK; Sorin Biomedical, Irvine, California, USA). The normal range sitting at rest and on a normal sodium diet was 0.2–2.8 ng/ml per h; intraassay and interassay coefficients of variation were within 8 and 10%, respectively. A cut-off upright PAC/PRA ratio (ARR) of less than 30, in the presence of aldosterone greater than 15ng/dl and suppressed PRA, was used as a screening test to exclude primary aldosteronism.

Cardiac Studies

All patients were evaluated with 2D-echocardiography, cardiac magnetic resonance (CMR) and invasive cardiac studies including coronary angiography and left ventricular EMB to clarify the etiology of cardiomyopathy, after written informed consent and approval by local ethical committee. Biopsy samples were processed for histology, electron microscopy, immunohistochemistry, and Western Blot analysis of myocardial aldosterone receptors and aquaporin 1.

Cardiac Magnetic Resonance

In all patients a standard CMR examination was performed with a 1.5-T system (Magnetom Avanto; Siemens Medical Systems, Germany) using a body and phased array coils. Scanning protocol consisted with the acquisition of TSE T2w-STIR, cine SSFP (steady-state free precession) and delayed enhancement (DE) sequences 12-18 minutes after gadolinium administration; on short-axis images left ventricle was completely encompassed from the base to the apex acquiring a

total of 10-12 images. T1 mapping imaging was also performed in all cases before and after contrast using a modified look-locker (MOLLI) sequence acquired in short axis at basal- mid and apical segments, before and after contrast. All CMR studies were analyzed in consensus by two experienced observers blinded of EMB results, using a workstation with dedicated cardiac software (cmr42© v.40, Circle Cardiovascular Imaging Inc.,Calgary, Canada).

Histology , electron microscopy and molecular studies

Five to eight endomyocardial biopsy samples each patient were cut and processed for routine histological analysis and for transmission electron microscopy (TEM). In those patients with inflammatory cardiomyopathy at histology, two frozen samples were processed for PCR for the most common cardiotropic viruses including adenovirus, enterovirus, Influenza A/B, Parvovirus B19, Cytomegalovirus, HHV6, HSV1, HSV2, EBV, HCV. In addition, two myocardial fragments each patient were processed for assessment of aldosterone receptors and aquaporin channels. For histological analysis the endomyocardial samples were fixed in 10% buffered formalin and paraffin embedded. Five micron-thick sections were stained with hematoxylin & eosin, Masson trichrome and Miller's Elastic Van Gieson. For TEM, samples were fixed in 2% glutaraldehyde in a 0.1 M phosphate buffer, at pH 7.3, post fixed in osmium tetroxide and processed following a standard schedule for embedding in Epon resin. Ultrathin sections were stained with uranyl-acetate replacement stain (EMS #22405, from EMS, Hatfield, Pa, USA) and lead hydroxide. A Jeol-1400-plusTEM was used for observation and photographic analysis.

Assessment of myocardial aldosterone receptors and aquaporin channels

Immunohistochemistry

The expression of aldosterone receptors (AR) and aquaporins (AQP) was evaluated by immunoperoxidase using mineralocorticoid receptor monoclonal anti-body (1:100, Enzo Life Sciences, Inc. 10 Executive Blvd Farmingdale, NY 11735 U.S.A.) and Aquaporin 1 (AQP1) mouse monoclonal antibody (1:80, Santa Cruz Biotechnology, Inc. 10410 Finnell Street Dallas, Texas 75220 U.S.A.) as primary antibodies. Intensity of immunostaining was semi quantitatively evaluated as absent (grade 0), weak (grade 1), mild (grade 2) moderate (grade 3), strong (grade 4). For each patient the grading was calculated on 10 different histological sections and the average value was computed.

Protein isolation and western blot

Heart tissue samples were treated as described (17). The expression of myocardial AR and AQP1 was visualized by using mineralocorticoid receptor monoclonal antibody (1:500), anti-Aqp1(1:100). Anti-α-sarcomeric actin (1:500, Sigma-Aldrich), antibody was used for normalization. Signal was visualized using a secondary horseradish peroxidase-labeled goat anti-mouse antibody (goat anti-mouse IgG-HRP 1:5000, SantaCruz Biotechnology) and enhanced chemiluminescence (ECL Clarity Bio-Rad). The purity as well as equal loading of the fraction was determined by measuring β-actin protein levels. Digital images of the resulting bands were quantified by the Image Lab software package (Bio-Rad Laboratories, Munchen, Germany) and expressed as arbitrary densitometric units.

Statistical analysis

Quantitative measurements are expressed as mean ± SD. A value of $p < 0.05$ was considered as significant. Normal distribution of variables was assessed with Kolmogorov–Smirnov test. Categorical data were presented as absolute frequencies and percent values. Difference between two groups was determined by unpaired t-test for continuous variables. The Fisher's exact test was used for comparison of categorical variables. Changes observed before and after immunosuppressive treatment were examined by paired t-test and McNemar test. Data analysis was performed using GraphPad Prism v6.04 for Windows (GraphPad Software).

Results

Twenty-six patients were included in the study; 20 were males (77%), median age was 58.4 ± 11.4 years. Comparison of baseline biochemical, clinical and endomyocardial biopsy data among patient population (Group A) and normal controls (Group B) are shown in Table 1.

Cardiac studies

Two-dimensional echocardiography showed a dilated left ventricle (LVEDD 61.5 ± 7.4 mm) with severely reduced ejection fraction (LVEF % 27.8 ± 5.8). Cardiac magnetic resonance (CMR) confirmed LV dilation (LVEDV 226.8 ± 69.6 mm) and dysfunction (LVEF % 26.3 ± 7.1) (figure 1, panel A-B). Areas of late gadolinium enhancement were detectable in the interventricular septum and infero-posterior LV wall in patients with dilated cardiomyopathy, alcoholic cardiomyopathy, diabetic cardiomyopathy and long-lasting inflammatory cardiomyopathy suggesting increased myocardial fibrosis. In patients with active myocarditis, CMR showed areas of late gadolinium enhancement (subepicardial, mid-wall, or diffuse) corresponding to myocardial edema on T2-weighted images and increased native T1 values on mapping. Coronary network was normal in all patients.

Endomyocardial biopsy studies and ultrastructural findings

Histological diagnosis was virus-negative inflammatory cardiomyopathy in 15 patients (57.7%), idiopathic non-familiar dilated cardiomyopathy in 6 patients (23.1%) and, in the remaining cases (19.2%) the etiology of heart failure was alcoholic cardiomyopathy (n=2) and diabetic cardiomyopathy (n=3) (18).

In all patient population histology showed an increased volume of cardiomyocytes, containing large intracellular vacuoles (vacuolar or hydropic degeneration) and a typical cell swelling (or cloudy swelling) as described by Virchow (19) (Figure 1 panels C-H, Supplemental Figures S1, S2 Panel A, S3, S11 and S17).

At TEM a number of subcellular changes were constantly present, all directly or indirectly related to the cell volume changes and water and ion accumulation. Table 3 summarizes these changes and their recovery after therapy.

Large vacuoles contained an electron-clear material mostly corresponding to the enlarged cisternae of endo/sarcoplasmic reticulum, Golgi apparatus and other subcellular compartments (Supplemental Figures S4-S17). Cytosol also appeared electron-clearly diluted with large regions of myofibrillolysis (Figure 1 panel D and Supplemental Figures S10-S11). Noteworthy, in most of myocardiocytes mitochondria were uniformly swollen (Figure 1 panel G) with highly diluted/vesiculated matrix and disorganized cristae; in other myocardiocytes their size may vary greatly, suggesting an abnormal dynamic in the fusion/fission process. Moreover, the distribution of mitochondria along the cell was highly irregular, being mostly grouped in large clusters, in contrast with columnar

arrangement seen in normal myocardium (Supplemental Figures S12-S17). Nuclear changes included swelling of nucleoplasma, chromatolysis, nucleolar disorganization and nuclear membrane alterations (Figure 1 panel F). Intercalated disk sometimes was focally disorganized and lateral myocardiocyte junctions appeared mostly disorganized by the increased spaces among cells (extracellular edema, Supplemental Figures S4-S7).

Importantly, in all these tissues AR, ion channels and transporters, and aquaporins have been explored in many other papers (20-32), suggesting their involvement in ion/water compartment changes.

Immuno-histochemistry for AR showed a lower grading in heart failure (Figure 2 panel A) because of aldosterone competitive binding (33); conversely western blot of aldosterone receptors showed 2.3 increase of protein expression (figure 2 panel C). Immunostaining for AQP1 was elevated (Figure 2 panel E) as well as western Blot of cardiomyocyte AQP1 that showed 2.6 fold increase in dysfunctional heart (Figure 2 panel F).

Treatment and follow up

All patients were treated according to the current heart failure guidelines of the European Society of Cardiology with betablockers, antagonists of renin-angiotensin system, mineralocorticoid/aldosterone receptor antagonists (spironolactone 25 mg daily), diuretics in case of congestion, and if needed, antiarrhythmic drugs (34). The fifteen patients with virus-negative inflammatory cardiomyopathy were treated with immunosuppressive therapy including prednisone 1 mg/kg per day for 4 weeks followed by 0.33 mg/kg per day for 5

months and azathioprine 2 mg/kg per day for 6 months according to TIMIC trial (16) in addition to standard therapy for heart failure. At the end of treatment, 8 of them accepted a control left ventricular EMB.

All patients were clinically followed up at 6 months with ECG, echocardiogram and CMR. As a consequence of optimized heart failure treatment, all patients showed an improvement in clinical status and better exercise tolerance. No patient died. In particular, LVEF in patients with dilated CM, alcoholic CM and diabetic raised from 23.4 ± 4.2 to 30.1 ± 5.9 %. Better metabolic control in diabetic patients and withdrawal from alcohol in diabetic patients contributed to clinical recovery.

Patients with virus-negative inflammatory cardiomyopathy showed a more pronounced clinical benefit after the immunosuppressive therapy with increase in LVEF (Table 2). Cardiac dimensions reduced at CMR (LVEDV baseline: 270.8 ± 51.9 mm; LVEDV at 6 month-follow up: 205.8 mm ± 42.7 mm) and LVEF % rose from 23.3 ± 5.2 to 52.6 ± 5.9 (figure 3 panels A-B). Moreover, myocardial edema was no longer detectable at CMR as well as late gadolinium enhanced images were attenuated. In patients who accepted a control biopsy, histology showed healed myocarditis with reduced volume of cardiomyocytes, disappearance of large vacuoles, and recovery from most alteration of subcellular compartments described above (Figure 3 panels C-D).

A detailed description of the recovery of each cell compartment is shown in Table 3.. In particular, electron micrographs show an advanced reorganization of the swollen altered myocardiocytes with a general recovery from swelling and vacuolar degeneration, an almost normal distribution among myofibrils of

mitochondria with an orthodox/dense energized conformation, recovering from swelling and vesiculation. Of note, Golgi apparatus hypertrophy suggests a role in the vesicular extrusion of water and ions (20,21,27). Vacuoles of autophagy and extrusion of exosomes are also frequently seen in recovering samples after therapy (Supplemental Figure S2); both autophagy and large vesicle extracellular release could be other mechanisms for recovering from changes induced by hyperaldosteronism.

Besides aldosterone receptors and aquaporin channels that were both equally over-expressed in heart failure, normalized after cardiac recovery (Figure 2 panels B, D, E, F).

Discussion

Abnormal aldosterone signaling has been recognized to adversely affect the cardiovascular system. On the other hand, contrast of aldosterone activity in the failing heart by aldosterone inhibitors has been found clinically beneficial being followed by reduction of left ventricular hypertrophy and decrease in mortality and cardiovascular-related hospitalizations compared with placebo (1-4). On the base of clinical studies, aldosterone inhibitors have been recommended by the current guidelines in the pharmacologic treatment of heart failure (5-6).

Nevertheless, the cellular and morpho-molecular basis of myocardial damage in failing heart due to secondary hyperaldosteronism and its recovery is still unknown.

In the present report, analyzing pre- and post-recovery endomyocardial biopsy samples, it has been documented that, in failing heart, increased plasma aldosterone activity is associated with over-expression of myocardial aldosterone receptors and aquaporin-1. In particular, at western blot analysis, both figures increased by more than 100 %.

Role of Aldosterone receptors

AR is a protein with two isoforms, one bound to plasma-membrane and the cytosolic one. The last one can dimerize and migrate to the nucleus acting as transcription factor. AR dimer is responsible for a complex gene expression, including ion transporters, co-transporters, and ion channels, especially some Na+ channels, allowing sodium entry into the cell (29, 35). Therefore, increased AR signaling may alter ion distribution between myocardiocytes and extracellular spaces, and in the cytoplasm among different subcellular compartments.

A transcriptional loop also activates the synthesis of new AR, according to western blot analysis (Figure 2 panel E).

Altering the ionic content of subcellular compartments and changing their osmolarity, the AVP2 (arginine/vasopressin receptor 2) is activated, producing AQP1 expression and increase of water movements along the osmotic gradient (20).

Role of Aquaporin-1

AQPs constitute a 13 members gene family of voltage-independent transmembrane channels which facilitate the movements of water across the

biological membranes, along the osmotic gradient. In the myocardium are present 3 AQPs: AQP1 the most expressed and AQ3 and AQP7 expressed to a lesser extent (13, 20). AQP1 is more abundant in the ventricles and less in the atria and in the vessel wall (endothelial cells), its subcellular localization in biological membranes may vary with trafficking among cell membranes and in relation to the function required.

Role of water and ion movements in damage production and its reversal.

In the present study, over-activation and over-expression of AR is hypothesized to cause transcription of Na+ channels (and potential-activated Cl-channels), producing an intracellular Na+ (and anions) inflow with increased cell osmolarity that activates AQ1 channels with consequent water mobilization (Figure 4). Water entrance into cardiac cells can be massive requiring its compartmentalization in vesicles, but it is also retained in the cytosol and particularly into the organelles including endoplasmic reticulum (Figure 1 panel D), mitochondria (Figure 1 panel G, H) and Golgi apparatus (Supplemetal figure S12, S15, S16). Cell nucleus appears affected as well by oedema that may be severe enough to induce focal chromatolysis (Figure 1 panel E). Accordingly, several previous papers (20-32) have demonstrated that vacuoles and cytosol swelling with electron-clear material are produced by massive movements of ions and water accumulating both in the cytosol (cloudy swelling) and/or segregated into vacuoles (vacuolar degeneration), strictly associated with alterations of cell volume control mechanisms. Not in the myocardium, but in several other tissues such as in kidney (23-25), liver (20,28), smooth muscle (29-31), lung (36), and duck salt gland (33).

Possible mechanisms involved in the ultrastructural recovery.

Although it is clear that after normalization of aldosterone signaling, the extrusion of ion and water is a relevant mechanism involved in the ultrastructural recovery of damaged myocardiocytes, ultrastructural evidence suggests that other mechanisms may be involved in the normalization of myocytes architecture and function. The table 3 summarizes the pathways which are active during the ultrastructural recovery, being directly or indirectly associated to the cell volume normalization. In particular, the recovery of osmolarity, the normalization of AQP and the restoration of mitochondrial coupling (transition from swollen to orthodox/energized conformation) are directly related to the extrusion of water and ion. Activation of autophagocytosis and extrusion of non digested/unwanted material may be secondary to the restoration of energy levels obtained in parallel with mitochondrial recovery. Finally, mitochondrial dynamics (distribution and fission/fusion) and sarcomere reorganization can be also related to the cytoskeletal restoration secondary to cell volume recovery, ion homeostasis and energy production (37,38).

In addition, morpho-molecular changes observed in our patient population with heart failure are similar to those described in cardiomyopathy associated to primary aldosteronism (7).

Pathophysiologic consequences of electrolytes and water cell inflow appear to be cardiomyocyte swelling and likely functional impairment. In particular, it is believed that intracellular electrolytes and water overloading might negatively influence myocyte relaxation and contraction contributing to an impairment of diastolic and systolic cardiac function.

In support of this interpretation, endomyocardial biopsies obtained after recovery of cardiac contractility, show reduction in size as well as normalization of cardiomyocyte composition in parallel with downregulation of cell receptors.

Noteworthy, cardiomyocyte oedema was independent from the cause of heart failure. Indeed, patients with myocarditis as well as subjects with various type of dilated cardiomyopathy manifested the same histologic and ultrastructural findings correlated with myocyte water accumulation.

Limitations of the Study

While the present study shows for the first time the structural myocardial changes associated with secondary aldosteronism, it is unable to quantify its impact in terms of impairment of cardiomyocyte relaxation and contraction as well as its potential role in the generation of cardiac electrical instability.

Further unanswered points are the quantification of structural and functional recovery inducible by aldosterone-inhibitors and what is their most appropriate dosage.

Further, likely experimental studies, analyzing cardiomyocyte structural and receptor changes following aldosterone-inhibitors administration in animals with induced heart failure, are necessary.

Conclusions

Human heart failure is associated with secondary states of hyperaldosteronism leading to over-activation of myocyte aldosterone and aquaporin that independently from the cause of cardiac dysfunction induce intracellular water overloading that may determine swelling and functional compromise of organelles which recovery may per se improve cardiac contractility.

Our data confirm the negative impact of aldosterone pathway activation in the failing heart and the potential benefit from administration of aldosterone inhibitors. The overexpression of aldosterone receptors in the secondary state of hyperaldosteronism associated with heart failure determines cellular swelling as a consequence of AQP1 expression with intracellular water accumulation and intracellular sodium retention causing elevated intracellular osmolarity. These alterations produce vacuolar degeneration of cardiomyocytes; the persistence of cellular swelling leads to disruption of calcium homeostasis and cellular damage.

Cardiac recovery is accompanied by down-regulation of hormonal receptors and normalization of cell structure and composition. This supports the therapeutic role of aldosterone inhibitors in heart failure. For quantification of morpho-molecular effects of aldosterone inhibitors and their ideal dosage, further studies are needed.

Funding

This work was supported by European Project ERA-CVD "Transnational Research Projects on Cardiovascular Diseases"(JTC 2016 IKDT-IGCM) and Italian Ministry of Health given to IRCCS Spallanzani (39).

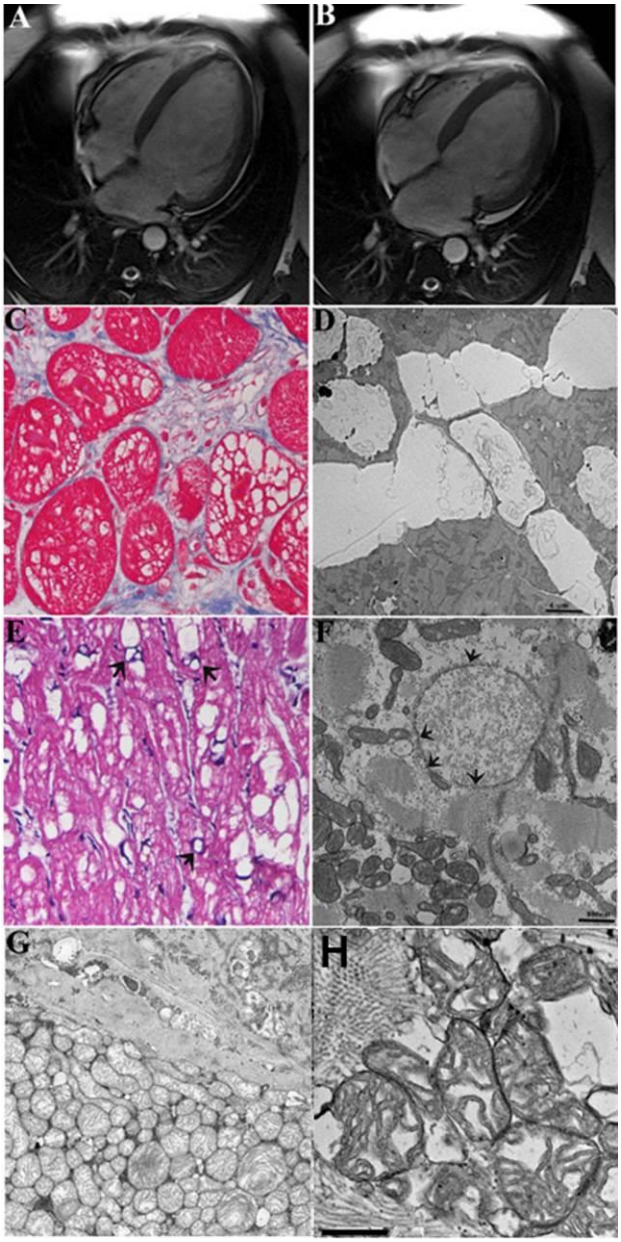

Figure 1: CMR, histologic and ultrastructural changes of cardiomyocytes in a 45-year old patient during heart failure caused by myocarditis.

Panels A-B: Cardiac magnetic resonance (CMR) showing bi-ventricular dilatation and severe dysfunction (LVEF 25%).

Panels C-H: LV endomyocardial biopsy showing vacuolar degeneration of myocytes (C) corresponding at electron microscopy to water accumulation in clear cisternae in the endoplasmic reticulum (D), nucleus (E-F,) and vesiculated

mitochondria (G-H). In panel F, remarkable nuclear edema causes chromatolysis and cell death; arrows indicate pores of nuclear membrane.

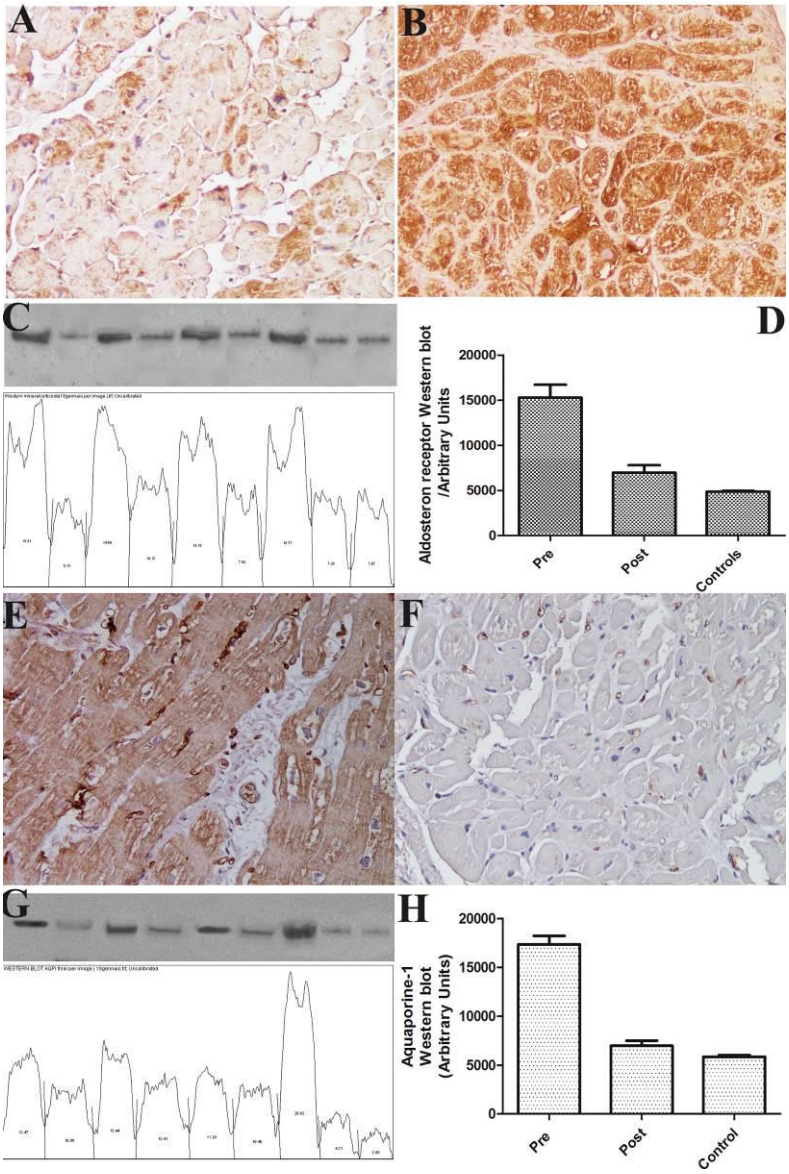

Figure 2. Immunostaining and western blot quantification of aldosterone and aquaporin 1 receptor under heart failure and after cardiac recovery.

Panels A-B: panel A shows reduced immunostaining for aldosterone receptors that remarkably increases (B) with enhancement (LVEF from 22 to 55%) of cardiac contractility.

Panels C-D: Western blot of aldosterone receptors showing **2.3** increase vs control during heart failure which returns to normal after normalization of cardiac function.

Panels E-F: Increased immunostaining for aquaporin 1 in dysfunctioning heart (E) that disappears (F) after cardiac recovery (200×).

Panel G-H: Western blot of cardiomyocyte aquaporin 1 receptors showing 2.6 fold increase (panel G) that declines after therapy.

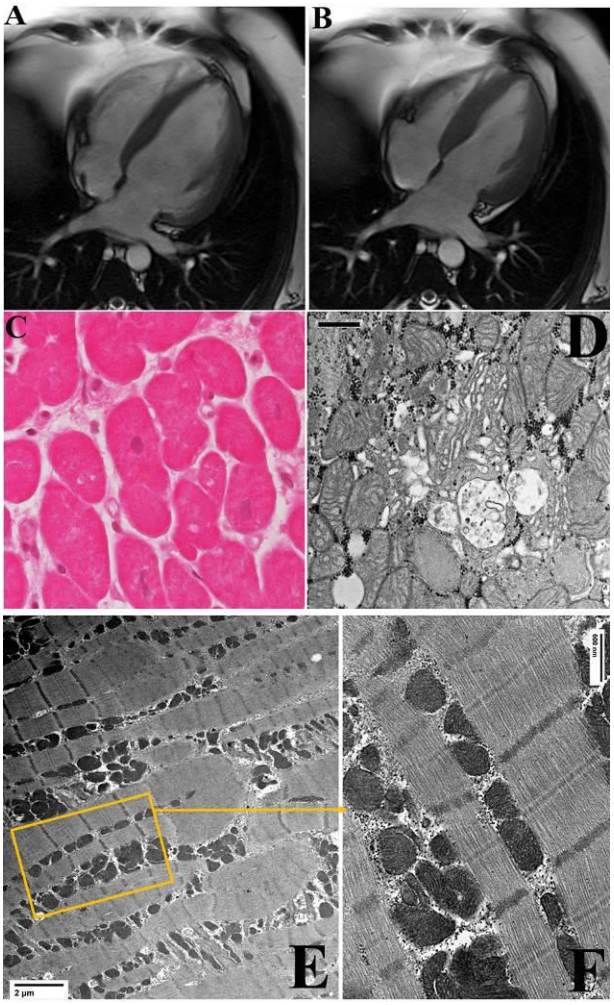

Figure 3: Clinical, histologic and ultrastructural changes of cardiomyocytes in the 45-year old patient with myocarditis presented in Fig 1, after cardiac recovery by immunosuppressive therapy.

Panels A.B: Control CMR documenting recovery of cardiac dimension and function with LVEF rising to 56%.

Panels C: Optical microscopy shows reduction of cardiomyocytes dimension with disappearance of vacuoles and decrease of extracellular spaces following cardiac recovery.

Panel D: Hypertrophic/hyperfunctioning Golgi apparatus with enlarged vesicles for water/ion extrusion.

Panel E-F: Recovery of ultrastructure with normal sarcomere and mitochondrial organization. Detail (F) shows energized mitochondria in columnar distribution among normal well organized sarcomeres.

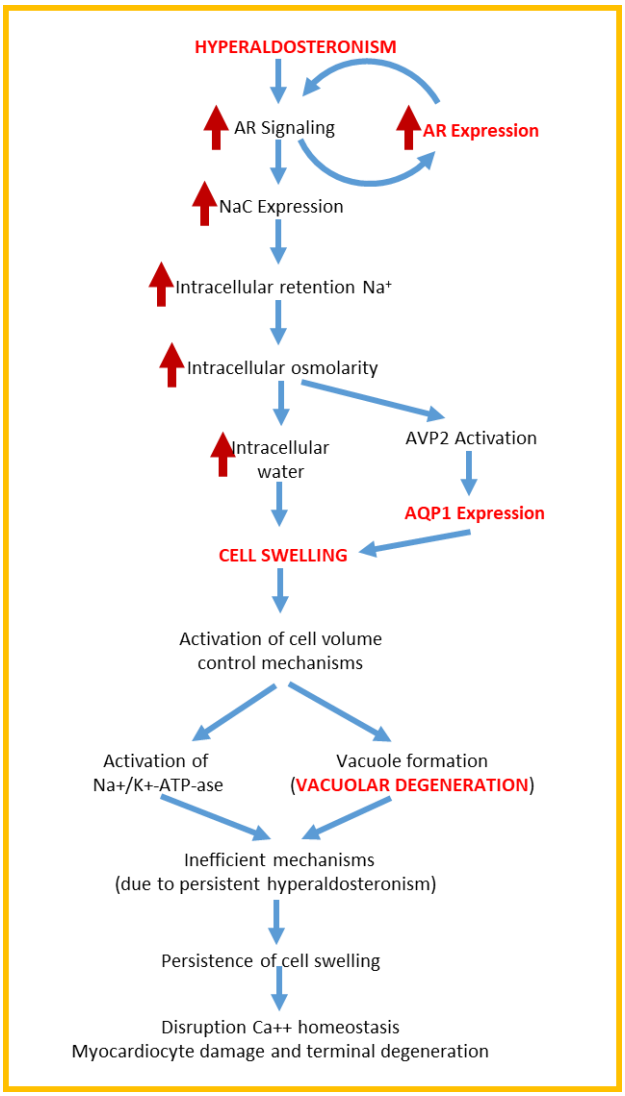

Figura 4. An hypothetical representation of the sequences triggered by aldosterone signaling leading to ion/water homeostasis disruption and to the myocardiocyte damage.

Table 1. Comparison of baseline biochemical, clinical and endomyocardial biopsy data among patients with human heart failure (Group A) and normal controls (Group B).

	Group A **n= 26**	**Group B** **n= 26**	**p value***
Age	58.4±11.4	57.5±11.5	0.818
Sex (M/F)	20M, 6F	17M, 9F	0.541
BMI (kg/m^2)	23.6±3.5	23.3±1.8	0.0759
SBP (mmHg)	114.6±15.2	111.9±9.1	0.9249
DBP (mmHg)	68.8±9.5	66.3±6.2	0.4204
HR (bpm)	79.1±12.8	74.5±5.5	0.4854
Blood values			
Creatinine (mg/dl)	1.3±0	0.9±0.2	0.01
Na (mmEq/L)	139.1±3.1	137.7±2.6	0.05
K(mmEq/L)	4.0±0.4	3.9±0.2	0.3032
Ca (mmEq/L)	10.0±0.4	9.2±0.4	0.2614
PAC (pg/ml)	185.4±68.7	61.6±16.1	0.05
PRA (pg/ml)	18.8±7.8	4.6±1.8	0.0001
PAC/PRA ratio	8.6±6.4	13.1±3.4	0.01
2d-Echocardiography			
MWT (mm)	11.0±2.6	9.6±0.9	0.01
LVEDD (mm)	61.5±7.4	44.4 ± 4.5	0.0001
LVEF%	27.8±5.8	59.7±4.2	0.0001

Cardiac Magnetic Resonance Imaging			
MWT (mm)	11.3±2.4	9.8±0.9	0.01
LVEDV (ml)	226.8±69.6	82.6±4.0	0.0001
LVESV (ml)	169.5±62.9	30.1± 4.2	0.0001
LVEF (%)	26.3±7.1	61.6±16.1	0.0001
LV mass (g)	187.5±70.1	87.8±19.2	0.0001
Endomyocardial biopsy studies			
Cardiomyocyte diameter (μm)	34.5±3.6	15.3 ± 2.5	0.0001
Fibrosis (%)	13.6±1.8	1.5 ± 0.46	0.0001
Aldosterone receptor grade (0/4)	1.6±0.8	2.9± 0.7	0.0001
AQP1 grade (0/4)	3.3±0.5	1.4 ± 0.3	0.0001
Aldosterone receptor Western blot (arbitrary units)	15543±3736	6712 ± 1352	0.01
AQP1 Western blot (arbitrary units)	17043±1648	6314 ± 851	0.01

*p values referred to comparison between three groups. p value <0.05 was considered statistically significant. Quantitative measurements are expressed as mean ± SD.

M=Male, F=Female, BMI= Body Mass Index, SBP= Systolic Blood Pressure, DBP= Diastolic Blood Pressure, HR= Heart rate, PAC=plasma aldosterone concentrations, PRA=plasma renin activity, PAC/PRA ratio=plasma aldosterone concentration/plasma renin activity, MWT=maximal wall thickness, LVEDD=left ventricular end-diastolic diameter, LVEF=left ventricular ejection fraction,

LVEDV=left ventricular end-diastolic volume, ## LVESV=left ventricular end-systolic volume, AQP1= aquaporin1, SR=sarcoplasmic reticulum, SD= standard deviation.

Table 2. Comparison of biochemical, clinical and endomyocardial biopsy data in 8 patients with heart failure baseline and at 6-month follow up.

	Baseline n= 8	**At 6-month FU n= 8**	**p value***
Age	**55.5±15.1**	**55.5±15.1**	
Sex (M/F)	6M, 2F	6M, 2F	
BMI (kg/m^2)	27.6±4.3	26.0±3.5	0.4
SBP (mmHg)	112.5±11.6	114.3±5.6	0.8294
DBP (mmHg)	67.5±7.1	71.6±3.4	0.1376
HR (bpm)	81±9.9	70.0±6.9	0.05
Blood values			
Creatinine (mg/dl)	1.1±0.1	0.8±0.2	0.05
Na (mmEq/L)	139.5±3.0	139.6±1.8	0.9577
K(mmEq/L)	4.1±0.25	4.0±0.1	0.7080
Ca (mmEq/L)	9.2±0.3	9.2±0.3	0.9575
PAC (pg/ml)	92.6±65.4	57.5±33.9	0.0830
PRA (pg/ml)	14.8±12.8	10.0±5.5	0.6454
PAC/PRA ratio	16.1±18.1	5.6±1.5	0.0582
2d-Echocardiography			
MWT (mm)	10.5±2	9.7±1.2	0.3506
LVEDD (mm)	61.5±7.4	54.8 ± 3.9	0.6731
LVEF%	26.2±3.7	51.6±5.8	0.0001
Cardiac Magnetic Resonance Imaging			
MWT (mm)	11.0±2.7	10.1±1.1	0.3601

LVEDV (ml)	270.8±59.7	205.8±42.7	0.05
LVESV (ml)	207.5±51.9	97.3± 13.7	0.0001
LVEF (%)	23.3±5.2	52.6±5.9	0.0001
LV mass (g)	160.7±46.6	139.2±37.4	0.3823
Endomyocardial biopsy studies			
Cardiomyocyte diameter (µm)	32.6± 1.9	23.5±2.6	0.0001
Fibrosis (%)	13.6±1.8	13.6±1.8	-
Aldosterone receptor grade (0/4)	1.5±0.4	3±0.5	0.0001
AQP1 grade (0/4)	3.4±0.3	1.3±0.4	0.0001
Aldosterone receptor Western blot (arbitrary units)	14197±3844	8754±3185	0.05
AQP1 Western blot (arbitrary units)	15952±2109	6327±1063	0.05

*p values referred to comparison between three groups. p value <0.05 was considered statistically significant. Quantitative measurements are expressed as mean ± SD.

M=Male, F=Female, BMI= Body Mass Index, SBP= Systolic Blood Pressure, DBP= Diastolic Blood Pressure, HR= Heart rate, PAC=plasma aldosterone concentrations, PRA=plasma renin activity, PAC/PRA ratio=plasma aldosterone concentration/plasma renin activity, MWT=maximal wall thickness, LVEDD=left ventricular end-diastolic diameter, LVEF=left ventricular ejection fraction, LVEDV=left ventricular end-diastolic volume, LVESV=left ventricular end-

systolic volume, AQP1= aquaporin1, SR=sarcoplasmic reticulum, SD= standard deviation.

Table 3. Transmission electron microscopy features before and after therapy in 8 patients with heart failure baseline and at 6-month follow up.

Features	Baseline	At 6-month follow up
Myocardiocyte axis	Increased	Decreased/normal
General swelling	evident	Recovered
Presence of large vesicles	Frequent	Absent
Sarcoplasmic reticulum	Dilated	Normal/partially recovered
Golgi cysternae	Irregularly dilated	Dilated (increased function)
Mitochondria	Swollen/vesculated	Orthodox/condensed /energized
Mitochondria dynamics	Abnormal fission/fusion	Apparently normal
Mitochondria distribution	Grouping	Mostly columnar
Intercalated disc	Occasionally disrupted	Apparently recovered
Lateral junctions	Disrupted	Recovered
Sarcomeres	Myofibrillolyisis	Recovered

Supplemental Figures showing

baseline transmission electron microscopy findings

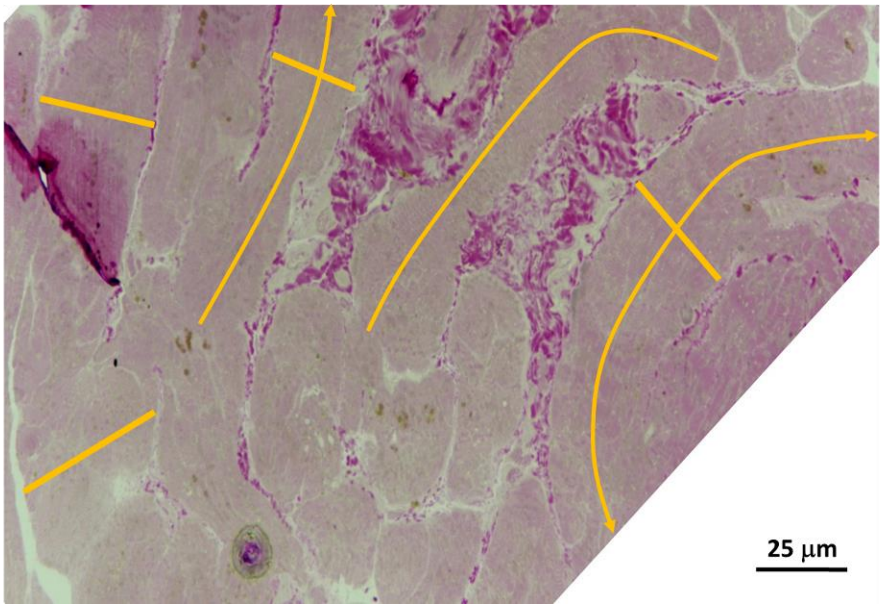

Supplemental Figure 1. Baseline left ventricular endomiocardial biopsy showing increased myocardiocyte axis and focal fibrosis.

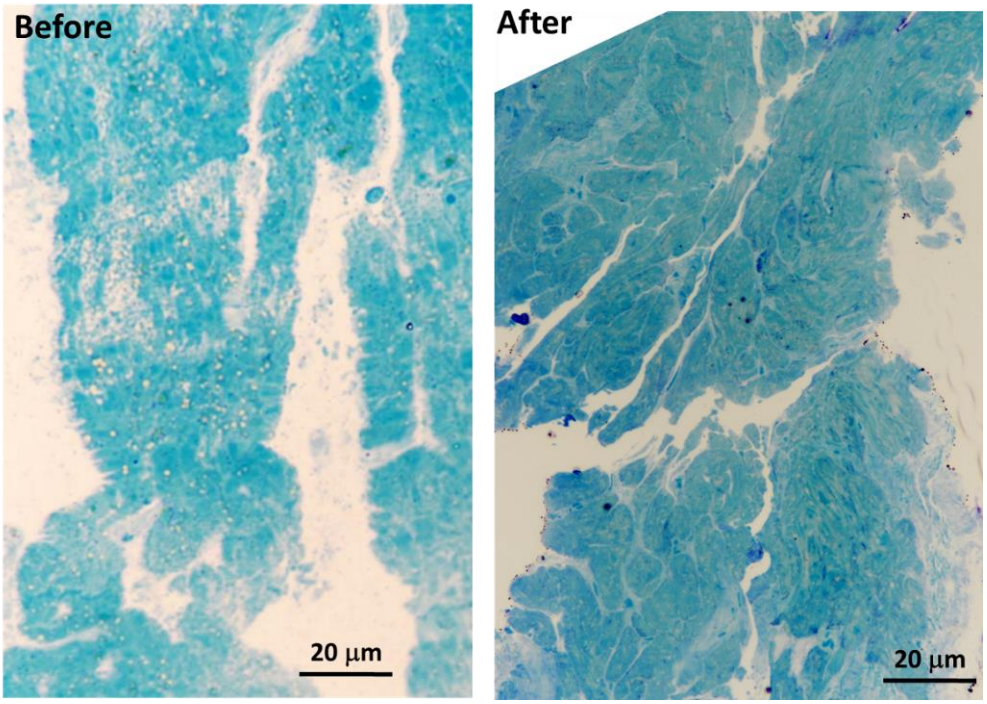

Supplemental Figure 2. Transmission electron microscopy showing vesiculation before and its recovery after therapy.

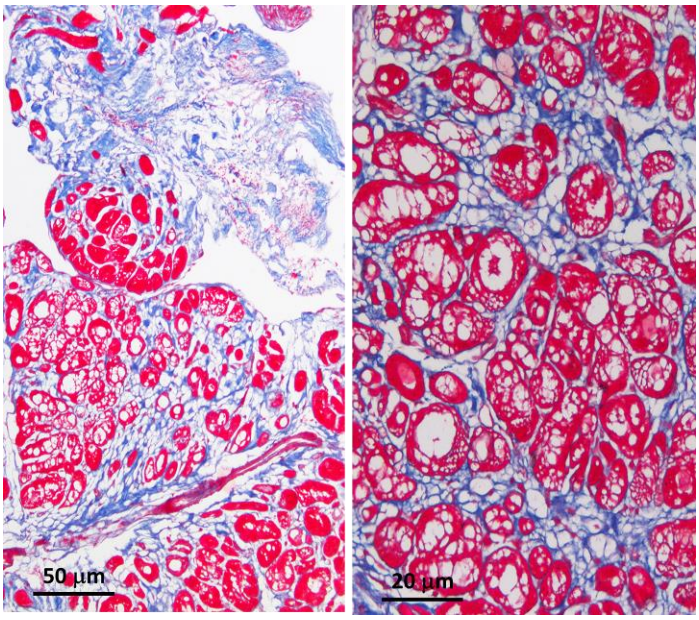

Supplemental Figure 3. Baseline left ventricular endomyocardial biopsy showing hypertrophy, large/small vesicles, increased extracellular space, fibrosis.

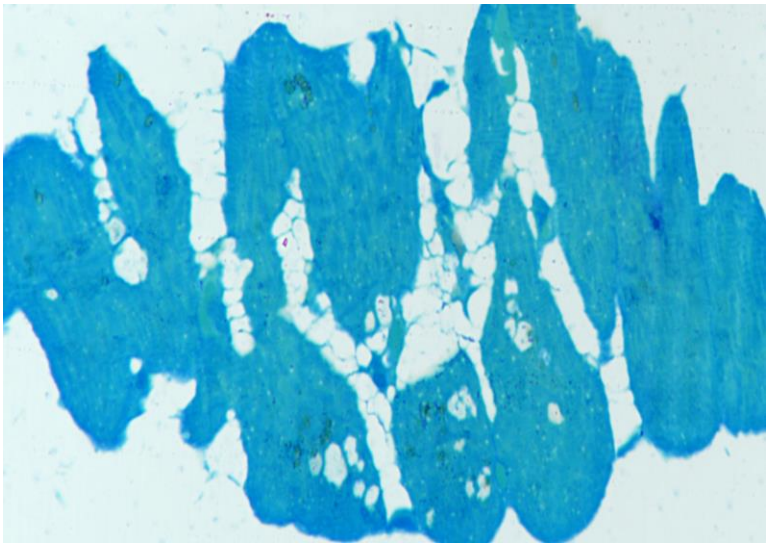

Supplemental Figure 4. Baseline transmission electron microscopy showing hypertrophy, large vesicles, increased extracellular space (plastic section, Azur II stained).

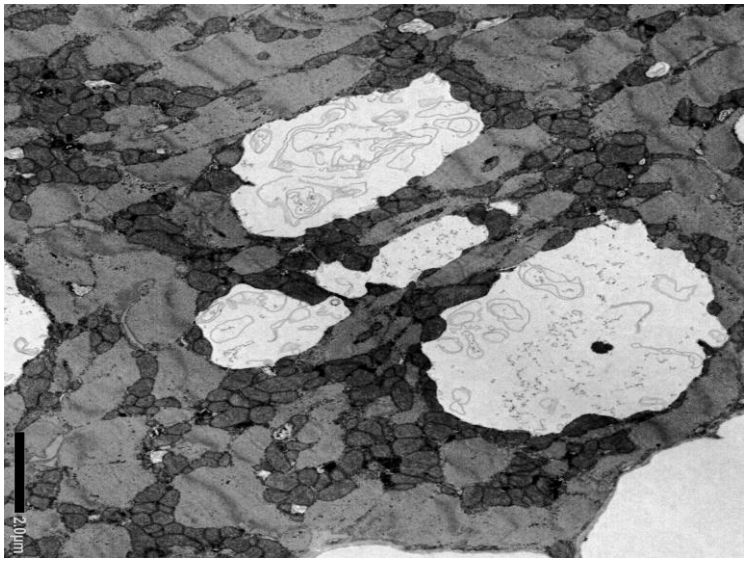

Supplemental Figure 5. Baseline transmission electron microscopy showing vacuolar degeneration: large intracellular vesicles with clear content.

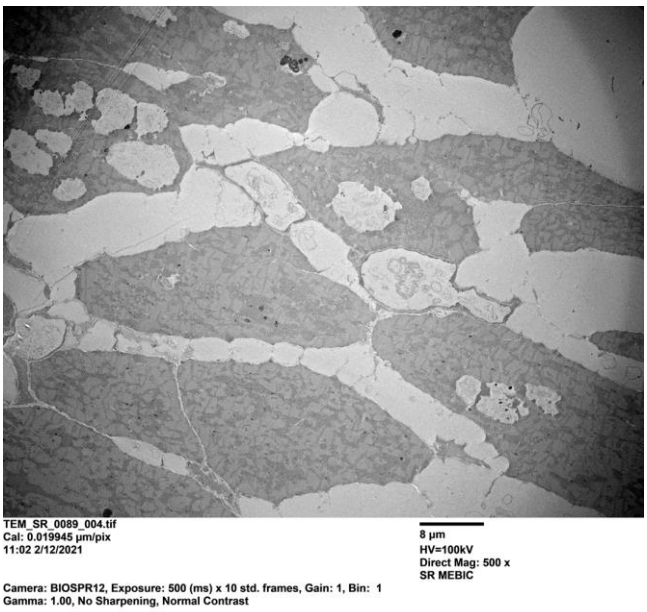

Supplemental Figure 6. Baseline transmission electron microscopy showing vacuolar degeneration: large intracellular vesicles with clear content, enlarged extracellular space with clear content (extracellular edema).

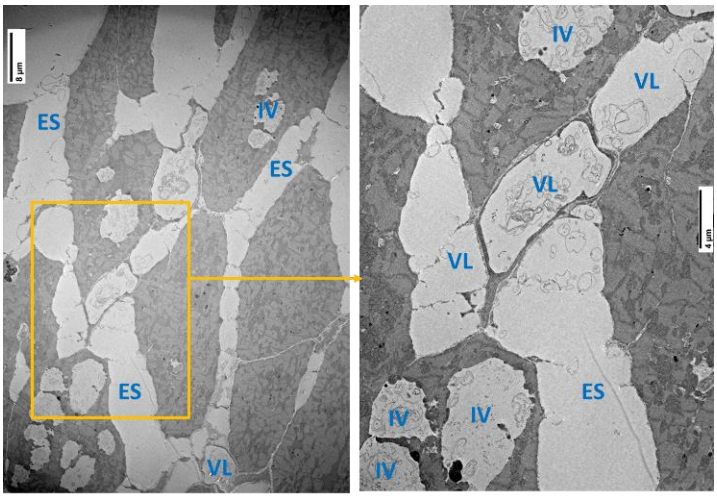

Supplemental Figure 7. Baseline transmission electron microscopy showing vacuolar degeneration: large intracellular vesicles (IV) with clear content and extracellular edema (large amount of extracellular fluids in extracellular spaces [ES] and vessel lumen [VL]).

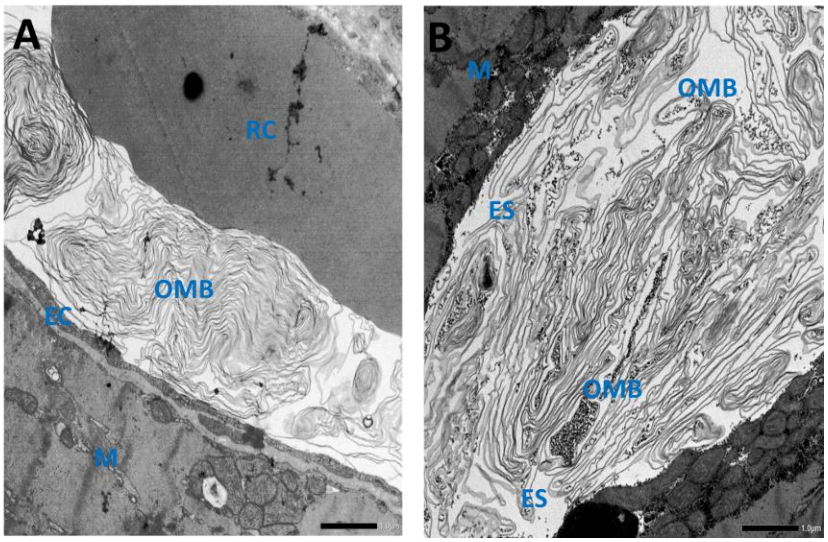

Supplemental Figure 8. Baseline transmission electron microscopy showing enlarged vessel lumen (VL) with osmiophilic myelin-like bodies (OMB), likely degenerating lipid membranes (A). Extracellular space also containing OMB (B). EC = endotheliall cells; RC = Red Cell; ES = Extracellular Space

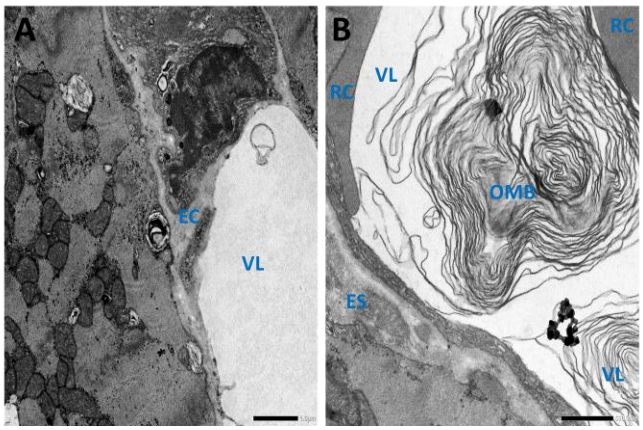

Supplemental Figure 9. Baseline transmission electron microscopy showing enlarged vessel lumen (VL) (A) with electron clear material and/or osmiophilic myelin-like bodies (OMB), likely degenerating lipid membranes (B). EC = endotheliall cells; RC = Red Cell; ES = Extracellular Space

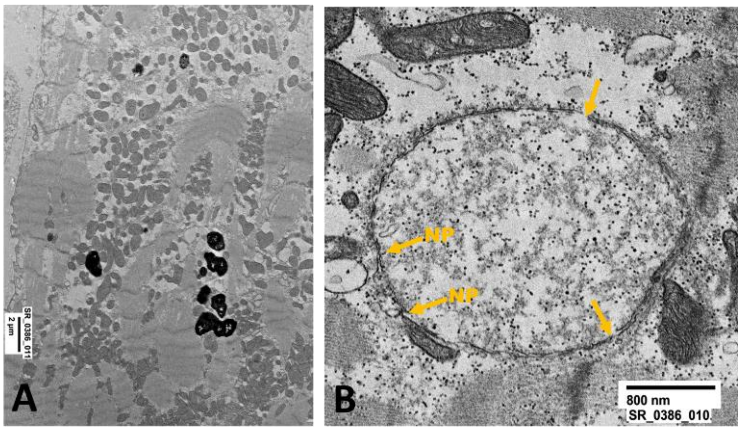

Supplemental Figure 10. Baseline transmission electron microscopy showing myofibrillolysis and chromatolysis with nuclear membrane damage.

A: Large areas of myofibrillolysis and sarcomere disorganization. Dense lipofiscin.

B: Nuclear damages: chromatolysis, nucleolar disorganization, nuclear membrane damages. NP = nuclear pore; Arrows = membrane fragmentation.

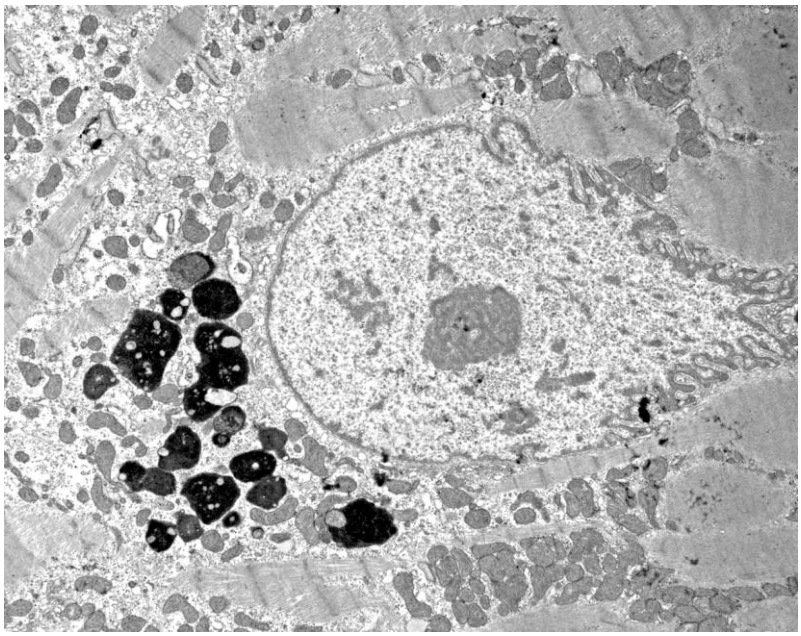

Supplemental Figure 11. Baseline transmission electron microscopy showing nuclear changes (chromatin fragmentation, abnormal nucleolonema) and cytoplasm changes (areas of myofibrillolysis, abnormal sarcomeres and accumulation of lipofuscins).

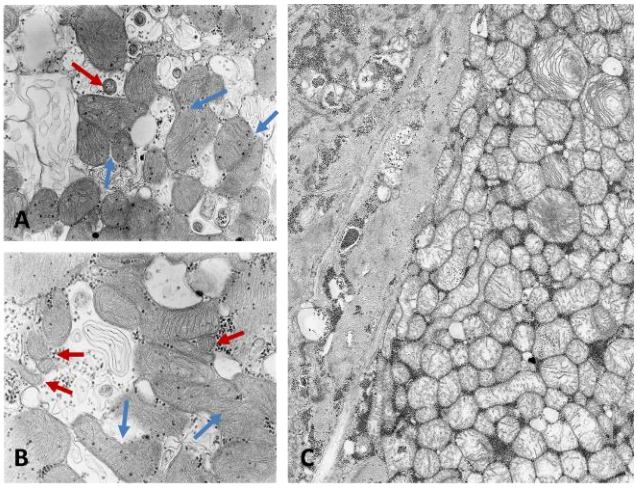

Supplemental Figure 12. Baseline transmission electron microscopy showing alterations of mitochondrial dynamics/conformation and small vesicles dilatation (sarcoplasmic reticulum, Golgi vesicles, lysosomes, mitochondria).

A-B. Evidences of altered fission/fusion dynamics, as shown by micro-mitochondria (red arrows) and fusing polymorphic/bizarre mitochondria (blu arrows). C. A group of densely packed swollen mitochondria. The matrix is electron clear, while cristae are plate-like conformation, although sometimes fragmented.

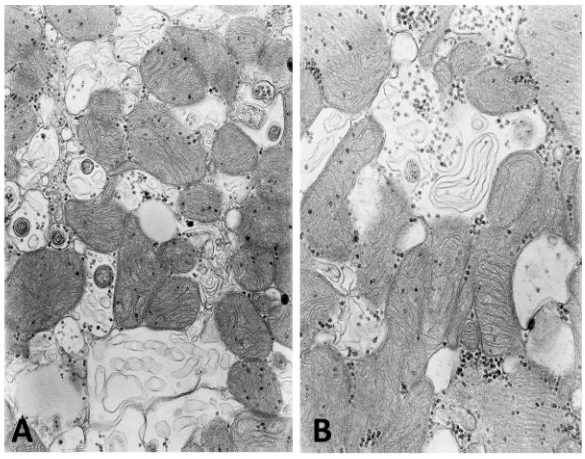

Supplemental Figure 13. Higher magnification of A and B electron panels of the figure 12.

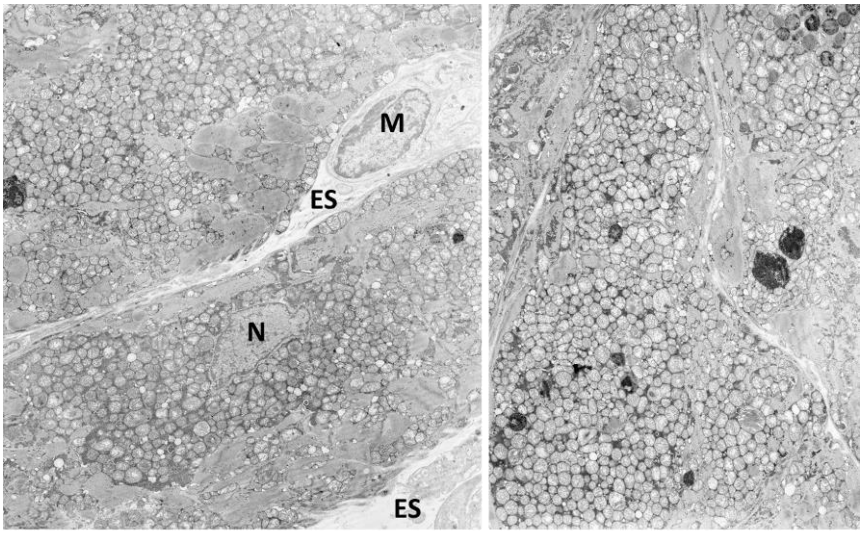

Supplemental Figure 14. Baseline transmission electron microscopy showing alterations of mitochondria.

Large groups of swollen mitochondria in a cytoplasm with reduced myofibrillar content and disorganized sarcomeres. Grouping of mitochondria may be responsible for an inefficient supply of high-energy phosphate molecules to the ATP-dependent functions, such as contraction. N = nucleus; ES = extracellular space; M = monocyte or large lymphocyte.

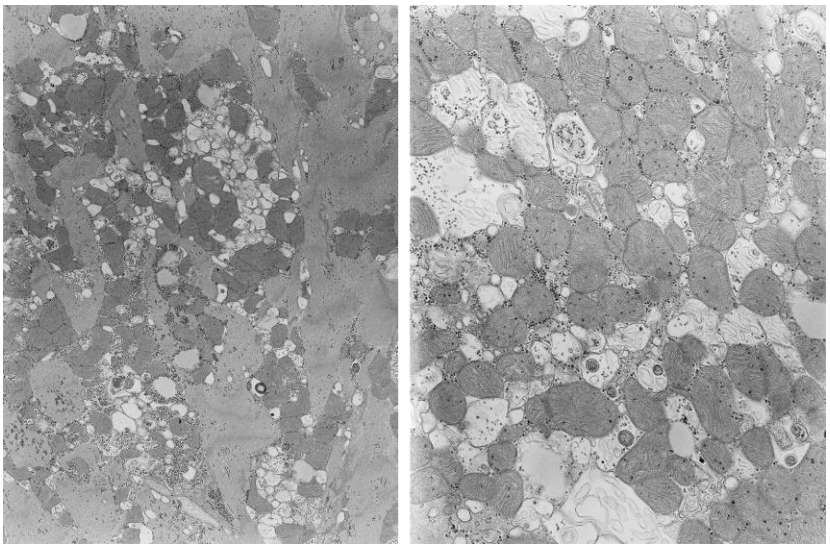

Supplemental Figure 15. Baseline transmission electron microscopy showing further details of dilated vesicles likely derived from sarcoplasmic reticulum, Golgi apparatus, lysosomes and other organelles.

The electron clear areas containing glicogen particles are either swollen cytosol or the lumen of a autophagocytic vacuole. Mitochondria are in orthodox/slightly swolle conformation.

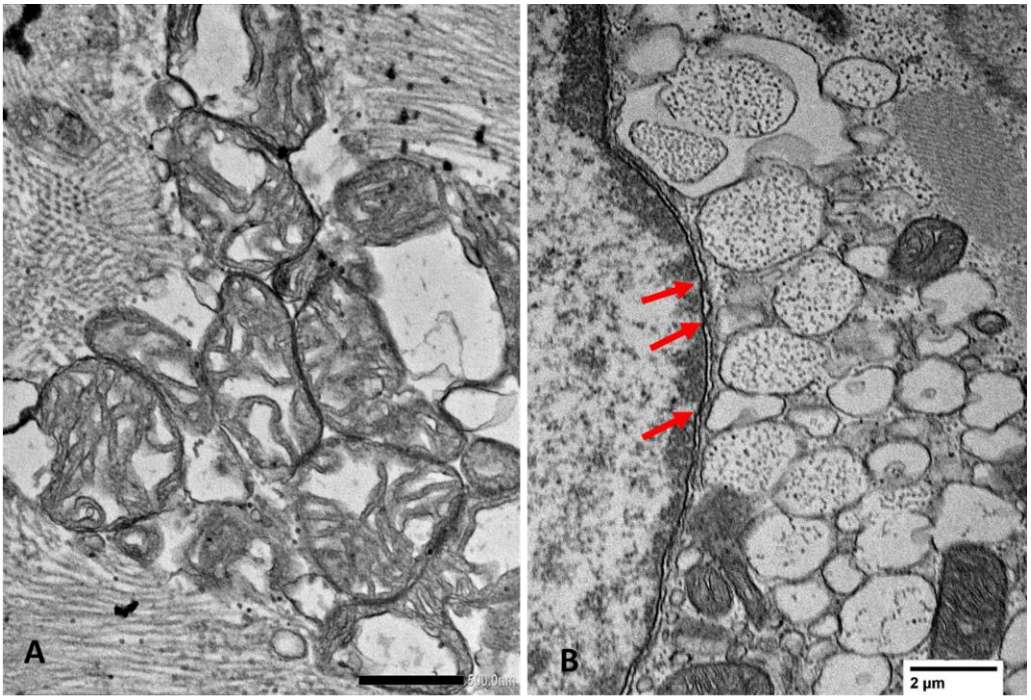

Supplemental Figure 16. Baseline transmission electron microscopy showing detail of highly swollen mitochondria and other organelles.

A. Detail of mitochondria: diluted and vesiculated matrix with irregular cristrae and damaged outer membrane

B. Detail small dilated vesicles of heterogeneous origin: phagosomes, autophagosomes, cyternae of sarcoplasmic reticulum (strictly interacting wit outer mitochondrial membrane) and, possibily, Golgi apparatus (close to nuclear membrane).

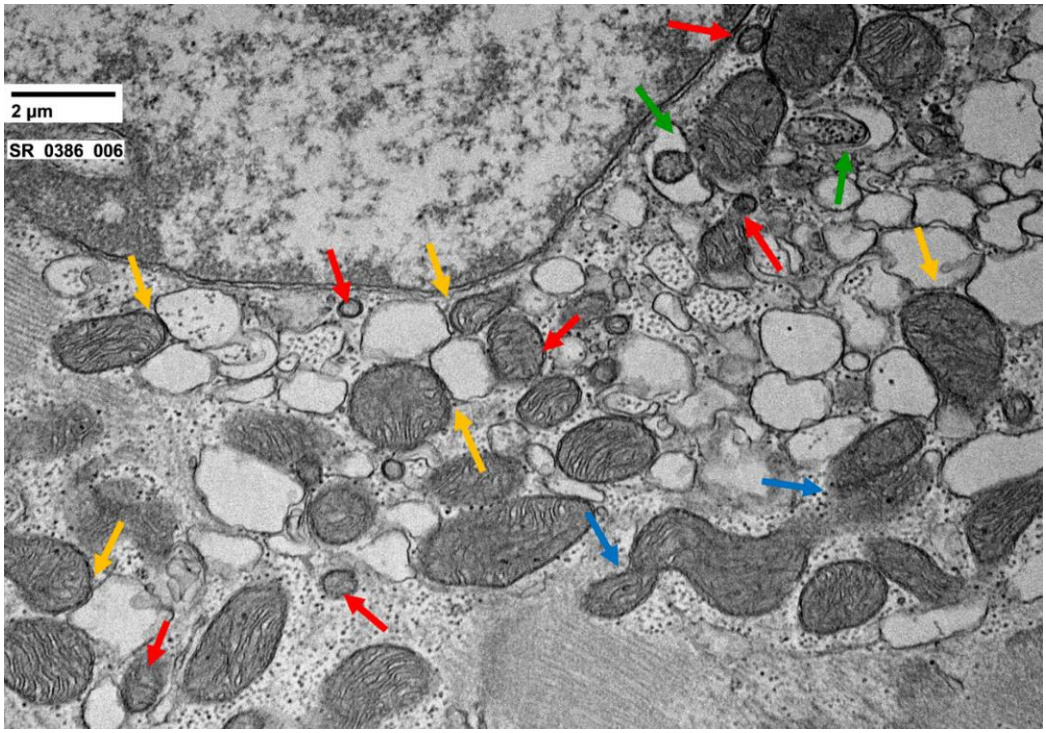

Supplemental Figure 17. Perinuclear region with small vesicles to that observed in the figure 16.

Electron microscopy showing a number of details of abnormal dynamics of mitochondria: micro-mitochondria (red arrows), bizarre fusion (blu arrows) close interaction with sarcoplasmic reticulum cysternae (orange arrows) and mitophagy (green arrows).

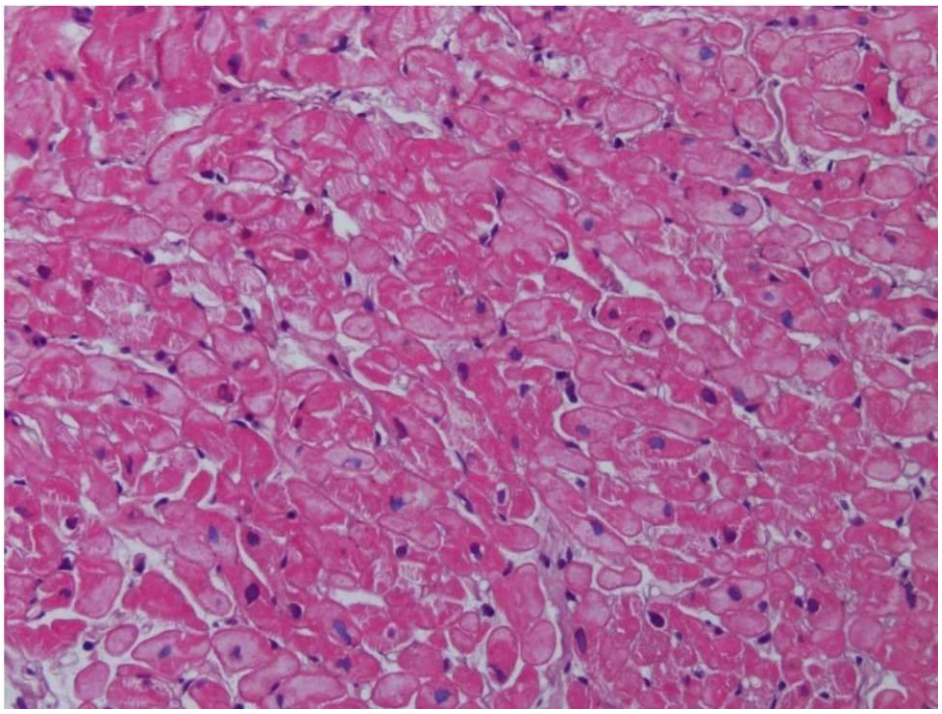

Supplemental Figure 18. Normal myocardium from EMB sample at histology

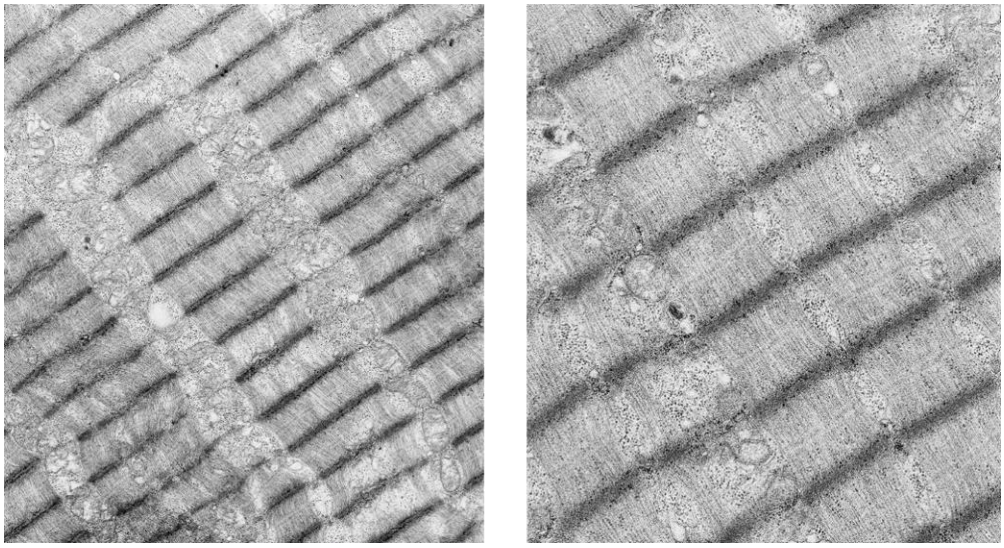

Supplemental Figure 19. Normal myocardium from a EMB sample at transmission electron microscopy

Index of figures

Index of tables

Index of supplemental figures

References

1. Emme WJ, Cody R, Castaigne A, Perez A, Palensky J, Wittes J. The effect of spironolactone on morbidity and mortality in patients with severe heart failure. N Engl J Med 1999;341: 709-717.

2. Pitt B, Remme W, Zannad F, Neaton J, Martinez F, Roniker B, Bittman R, Hurley S, Kleiman J, Gatlin M. Eplerenone, a selective aldosterone blocker, in patients with left ventriculardysfunction after myocardial infarction. N Engl J Med 2003;348:1309-1321.

3. Pitt B, Bakris G, Ruilope LM, Di Carlo L, Mukherjee R, EPHESUS investigators. Serum potassium and clinical outcomes in the eplerenone post-acute myocardial infarction and heart failure efficacy and survival study (EPHESUS). Circulation 2008;118:1643-1650.

4. Zannad F, McMurray JJ, Krum H, McMurray JJ, Swedberg K, Van Veldhuisen DJ, Vincent J, Pitt B, Zannad F. Eplerenone in patients with systolic heart failure and mild symptoms. N Engl J Med 2011;364:11-21.

5. Yancy CW, Jessup M, Bozkurt B, Butler J, Casey DE Jr, Drazner MH, Fonarow GC, Geraci SA, Horwich T, Januzzi JL, Johnson MR, Kasper EK, Levy WC, Masoudi FA, McBride PE, McMurray JJ, Mitchell JE, Peterson PN, Riegel B, Sam F, Stevenson LW, Tang WH, Tsai EJ, Wilkoff BL. 2013 ACCF/AHA guideline for the management of heart failure. Circulation 2013;128:1-375.

6. Yancy CW, Jessup M, Bozkurt B, Butler J, Casey DE Jr, Colvin MM, Drazner MH, Filippatos G, Fonarow GC, Givertz MM, Hollenberg SM,

Lindenfeld J, Masoudi FA, McBride PE, Peterson PN, Stevenson LW, Westlake C. 2016 ACC/AHA/HFSA update on new pharmacological therapy for heart failure: an update of the 2013 ACCF/AHA guideline for the management of heart failure. Circulation 2016;134:1-18.

7. Frustaci A, Letizia C, Verardo R, Grande C, Francone M, Sansone L, Russo MA, Chimenti C. Primary aldosteronism-associated cardiomyopathy: Clinical-pathologic impact of aldosterone normalization. Int J Cardiol. 2019 Oct 1;292:141-147. doi: 10.1016/j.ijcard.2019.06.055.

8. Coelho-Filho OR, Shah RV, Neilan TG, Mitchell R, Moreno H, Kwong R, JeroschHerold M. Cardiac magnetic resonance assessment of interstitial myocardial fibrosis and cardiomyocyte hypertrophy in hypertensive mice treated with spironolactone. J Am Heart Assoc. 2014;3:e000790. DOI: 10.1161/JAHA.114.000790.

9. Brown NJ. Contribution of aldosterone to cardiovascular and renal inflammation and fibrosis. Nat Rev Nephrol. 2013 August; 9(8): 459–469. doi:10.1038/nrneph.2013.110.

10. Brilla CG, Weber KT. Mineralocorticoid excess, dietary sodium, and myocardial fibrosis. J Lab Clin Med (1992) 120:893–901.

11. Cannavo A, Liccardo D, Eguchi A, et al Myocardial Pathology induced by aldosterone is dependent on non-canonical activities of G protein-coupled receptor kinases. Nature comm., 2016, 7:10877.

12. Russo MA, Morgante E, Russo A, van Rossum GD, Tafani M. Ouabain-Induced Cytoplasmic Vesicles and Their Role in Cell Volume Maintenance . Biomed Res Int 2015;2015:487256.
13. Rutkovskiy A, Valen G, Vaage J. Cardiac acquaporins. Basic Res Cardiol. 2013 Nov;108(6):393. doi: 10.1007/s00395-013-0393-6.
14. Rutkovskiy A, Mariero LH, Nygård S, Stensløkken KO, Valen G, Vaage J. Transient hyperosmolality modulates expression of cardiac aquaporins. Biochem Biophys Res Commun. 2012 Aug 17;425(1):70-5. doi: 10.1016/j.bbrc.2012.07.052.
15. Cooper LT, Baughman KL, Feldman AM, Frustaci A, Jessup M, Kuhl U, Levine GN, Narula J, Starling RC, Towbin J, Virmani R; American Heart Association; American College of Cardiology; European Society of Cardiology. The role of endomyocardial biopsy in the management of cardiovascular disease: a scientific statement from the American Heart Association, the American College of Cardiology, and the European Society of Cardiology. Circulation. 2007;116:2216 2233.
16. Frustaci A, Russo MA, Chimenti C. Randomized study on the efficacy of immunosuppressivetherapy in patients with virus-negative inflammatory cardiomyopathy: the TIMIC study. Eur Heart J 2009;30:1995–2002.
17. Chimenti C, Verardo R, Scopelliti F, Grande C, Petrosillo N, Piselli P, De Paulis R, Frustaci A. Myocardial expression of Toll-like receptor 4 predicts the response to immunosuppressive therapy in patients with virus-negative chronic inflammatory cardiomyopathy. Eur J Heart Fail. 2017 Jul;19(7):915-925.

18. Frustaci A, Ciccosanti F, Chimenti C, Nardacci R, Corazzari M, Verardo R, Ippolito G, Petrosillo N, Fimia GM, Piacentini M. Histological and proteomic profile of diabetic versus non-diabetic dilated cardiomyopathy. Int J Cardiol. 2016 Jan 15;203:282-9. doi: 10.1016/j.ijcard.2015.10.119).

19. Virchow Rudolf: Die Cellularpathologie in ihrer Begründung auf physiologische und pathologische Gewebelehre. Berlin, 1858.

20. Russo MA, Morgante E, Russo A, van Rossum GDV, and Tafani M. Ouabain-Induced Cytoplasmic Vesicles and Their Role in Cell Volume Maintenance. Biomed Res Int. 2015;2015:487256. doi: 10.1155/2015/487256.

21. Russo MA, Van Rossum GD, Galeotti T. Observations on the regulation of cell volume and metabolic control in vitro; changes in the composition and ultrastructure of liver slices under conditions of varying metabolic and transporting activity. J Membr Biol. 1977 Mar 8;31(3):267-99. doi: 10.1007/BF01869409.

22. Russo MA, Conforti A. Subcellular reactions to injury. I. Ultrastructural and biochemical investigations on the hepatic cellular damage produced by haemorrhagic shock in dogs. J Pathol. 1977 Feb;121(2):107-13. doi: 10.1002/path.1711210207.

23. Van Rossum GD, Russo MA. Ouabain-resistant mechanism of volume control and the ultrastructural organization of liver slices recovering from swelling in vitro. J Membr Biol. 1981 Apr 30;59(3):191-209. doi: 10.1007/BF01875425.

24. Van Rossum GDV, Ernst SA and Russo MA. Relative effects of furosemide and ethacrynic acid on ion transport and energy metabolism in slices of rat kidney cortex. Naunyn Schmiedebergs Arch Pharmacol. 1981 Aug;317(1):90-6. doi: 10.1007/BF00506264.

25. Van Rossum and Russo MA. Requirement of Cl- and Na+ for the ouabain-resistant control of cell volume in slices of rat liver. J Membr Biol. 1984;77(1):63-76. doi: 10.1007/BF01871101.

26. Russo MA, van Rossum GDV and Ernst SA. Morphological studies of rat kidney cortex slices undergoing swelling and its reversal: a possible basis for ouabain-resistant control cell volume. J Membr Biol. 1985;85(1):1-24. doi: 10.1007/BF01872002.

27. Van Rossum GDV, Russo MA and Schisselbauer JC. Role of cytoplasmic vesicles in cell volume maintenance. In Cell Volume Control. Part A: Volume control in isosmotic conditions, Gilles et al., edts., chapter II. Academic Press, Orlando, 1987.

28. Russo MA, Morgante E, Tafani M, van Rossum GD. Effects of medium calcium, and agents affecting cytoskeletal function, on cellular volume and morphology in liver tissue in vitro. J Cell Biochem. 2012 Jun;113(6):1915-25. doi: 10.1002/jcb.24060.

29. Shi XL, Wang GL, Zhang Z, Liu YJ, Chen JH, Zhou JG, Qiu QY, Guan YY.Alteration of volume-regulated chloride movement in rat cerebrovascular smooth muscle cells during hypertension. Hypertension. 2007 Jun;49(6):1371-7.Doi :10.1161/HYPERTENSIONAHA.106.084657.

30. O'Donnell ME, Owen NE. Sodium cotransport in vascular smooth muscle cells. Blood Vessels. 1991;28(1-3):138-46. doi: 10.1159/000158853. PMID: 1848123.

31. Tseng H, Berk BC. The Na/K/2Cl cotransporter is increased in hypertrophied vascular smooth muscle cells. J Biol Chem. 1992 Apr 25;267(12):8161-7. PMID: 1569072.

32. Van Rossum GDV, Russo MA and Schisselbauer JC. Role of cytoplasmic vesicles in cell volume maintenance. In Cell Volume Control. Part A: Volume control in isosmotic conditions, Gilles et al., edts., chapter II. Academic Press, Orlando, 1987.

33. Lombès M, Oblin ME, Baulieu EE, Farman N, Bonvalet JP. Immunohistochemical and biochemical evidence for a cardiovascular mineralcorticoid receptor. Circ Res 1992; 71: 503-510.

34. McDonagh TA, Metra M, Adamo M, Gardner RS, Baumbach A, Böhm M, Burri H, Butler J, Čelutkienė J, Chioncel O, Cleland JGF, Coats AJS, Crespo-Leiro MG, Farmakis D, Gilard M, Heymans S, Hoes AW, Jaarsma T, Jankowska EA, Lainscak M, Lam CSP, Lyon AR, McMurray JJV, Mebazaa A, Mindham R, Muneretto C, Francesco Piepoli M, Price S, Rosano GMC, Ruschitzka F, Kathrine Skibelund A; ESC Scientific Document Group. 2021 ESC Guidelines for the diagnosis and treatment of acute and chronic heart failure.Eur Heart J. 2021 Sep 21;42(36):3599-3726. doi: 10.1093/eurheartj/ehab368.

35. Hellal-Levy C, Fagart J, Souque A, Rafestin-Oblin ME. Mechanistic aspects of mineralocorticoid receptor activation. Kidney Int. 2000 Apr;57(4):1250-5. doi: 10.1046/j.1523-1755.2000.00958.x.

36. Mariani MF, Thomas L, Russo MA, and Van Rossum GDV: Regulation of cellular water and ionic content in lungs of fetal and adult rats. Exper Physiol, 76:745-763, 1991.

37. Van Rossum GDV, Ernst SA and Russo MA. Relative effects of furosemide and ethacrynic acid on ion transport and energy metabolism in slices of rat kidney-cortex. Naunyn-Schmiedeberg's Arch.Pharmacol., 317, (1981), 90-96.

38. Russo MA and van Rossum GDV: On the basis for cellular damage induced by ethacrynic acid in liver slices in vitro. comparison of structure and function. Lab.Invest., 54, (1986), 695-707.

39. Frustaci A, Letizia C, Chimenti C, Verardo R, Alfarano M, Scialla R, Bagnato G, Miraldi F, Sansone L, Russo MA. Myocardial Aldosterone Receptor and Aquaporin 1 Up-Regulation Is Associated with Cardiomyocyte Remodeling in Human Heart Failure. J Clin Med. 2021 Oct 22;10(21):4854. doi: 10.3390/jcm10214854.